

N-Substituted Amine-Borane Ionic Liquids as Fluid Phase Hydrogen Storage Materials

Brian D. Rekken, Asa E. Carre-Burritt, Brian L. Scott, Benjamin L. Davis*

Electronic Supporting Information

The ESI† contains:

- S2. List of compounds
- S3. ^1H , ^{11}B NMR spectra for N-ABILs 1-10 (**4a**, **5a**, **4b**, **5b**, **4c**, **5c**, **6c**, **4d**, **5d**, **4e**)
- S14. Table of dehydrogenation onset/max peak and integrated energy for N-ABILs 1-10 (**4a**, **5a**, **4b**, **5b**, **4c**, **5c**, **6c**, **4d**, **5d**, **4e**)
- S15. Head-space analysis (IR Spectra, MS) from the dehydrogenation of compound **6c** and **6c** + 2 AB
- S18. ESI-Mass spectra of compounds, **4a**, **6c**, and **4e**, as well as the post dehydrogenation product of **6c**
- S21. X-ray crystallographic data, collection parameters, and thermal ellipsoid plots for **2a**, **3b**, and **5a**
- S24. Crystallographic Methods

List of compounds

1. ClCH₂CH₂CH₂N(SiMe₃)₂
- 2a. [MImEtN(SiMe₃)₂]Cl
- 3a. [MImEtNH₃]Cl₂
- 4a. [MImEtNH₂BH₃]Cl
- 5a. [MImEtNH₂BH₃]OTf
- 2b. [EImEtN(SiMe₃)₂]Cl.
- 3b. [EImEtNH₃]Cl₂.
- 4b. [EImEtNH₂BH₃]Cl.
- 5b. [EImEtNH₂BH₃]OTf.
- 7b. [EImEtNH₂]Cl.
- 2c. [EImPrN(SiMe₃)₂]Cl.
- 3c. [EImPrNH₃]Cl₂.
- 4c. [EImPrNH₂BH₃]Cl.
- 5c. [EImPrNH₂BH₃]OTf.
- 6c. [EImPrNH₂BH₃]NTf₂
- 2d. [MPyroPrN(SiMe₃)₂]Cl.
- 3d. [MPyroPrNH₃]Cl₂.
- 4d. [MPyroPrNH₃BH₃]Cl.
- 5d. [MPyroPrNH₃BH₃]OTf.
- 7d. [MPyroPrNH₂]Cl.
- 3e. [MPyraPrNH₃]Cl₂.
- 4e. [MPyraPrNH₃BH₃]Cl.
- 7e. [MPyraPrNH₂]Cl.

2. ^1H and ^{11}B NMR spectra for N-ABILs 1-10 (4a, 5a, 4b, 5b, 4c, 5c, 6c, 4d, 5d, 4e)

^{11}B NMR spectra for the dehydrogenation products were processed on the MestReNova software ver. 9.0 using the Savitzky-Golay method with a Whittaker Smoother baseline correction.

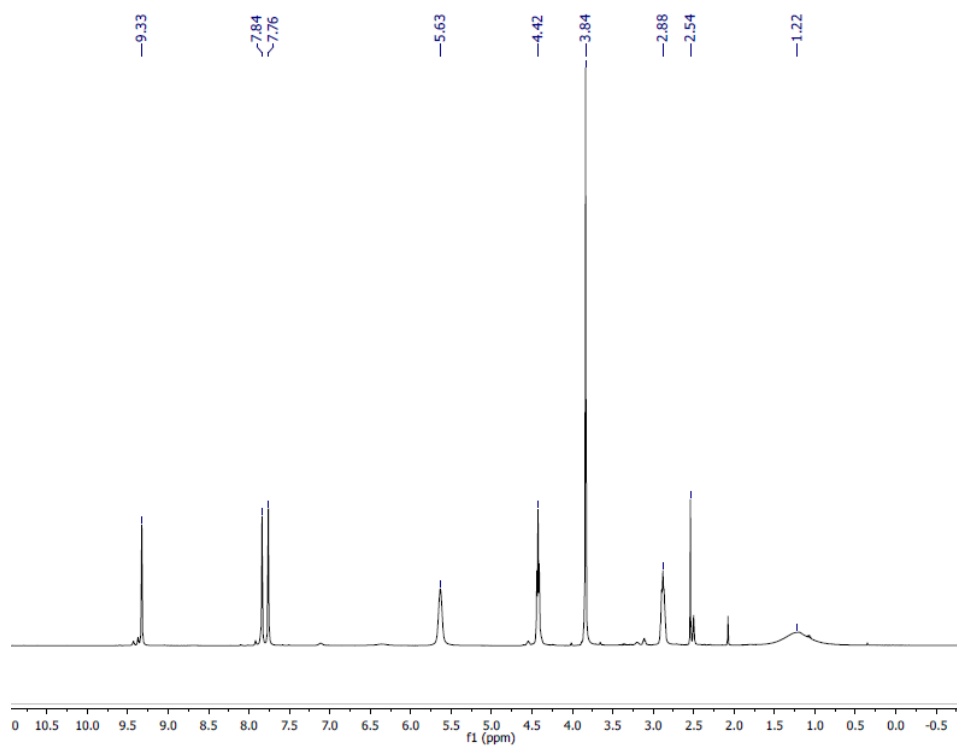


Fig S1. ^1H NMR spectrum of **4a**.

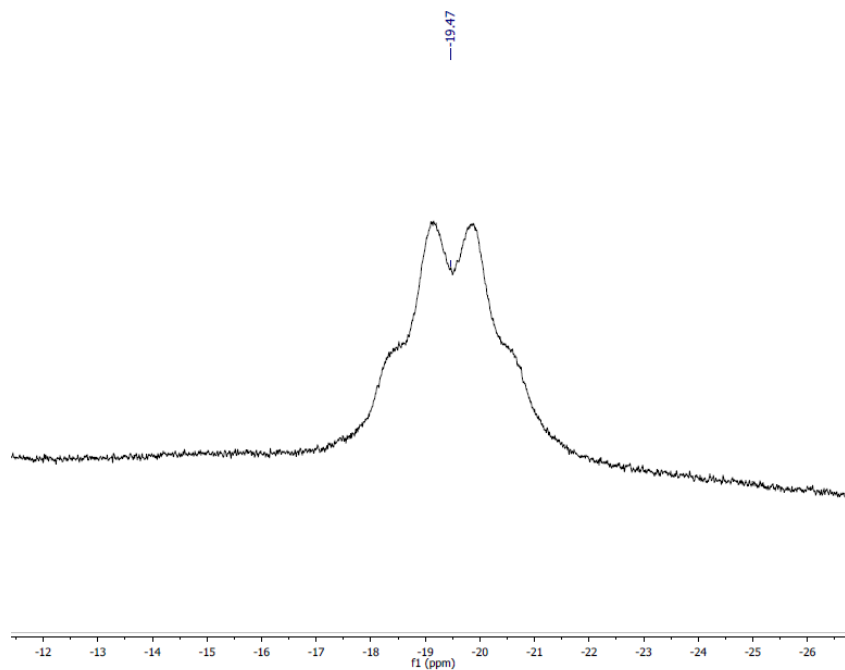


Fig S2. ^{11}B NMR spectrum of 4a.

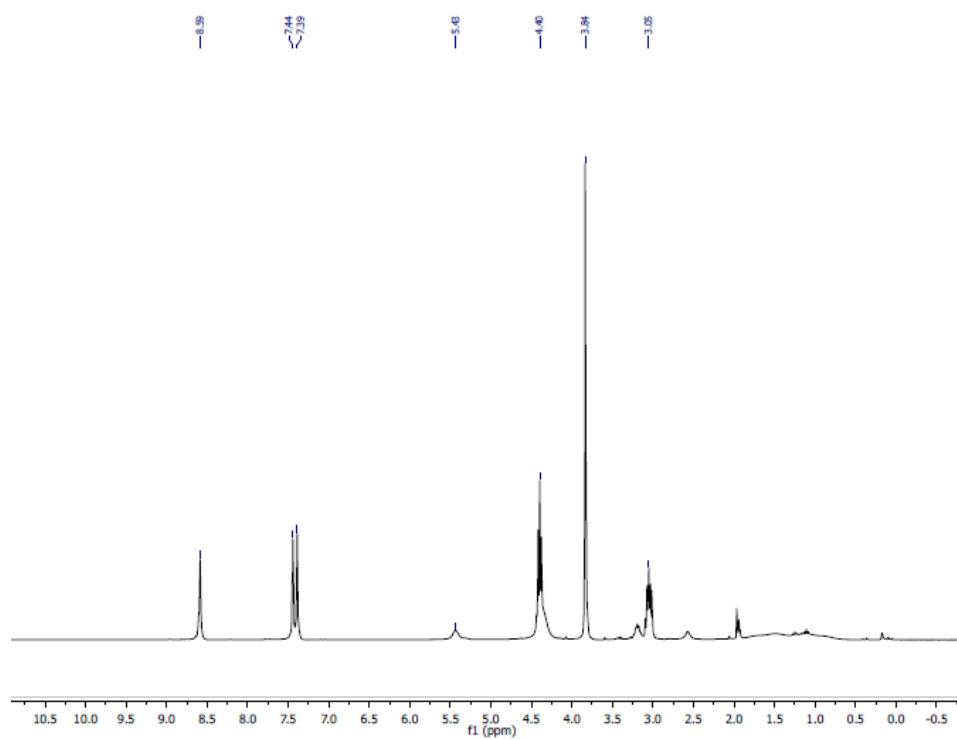


Fig S3. ^1H NMR spectrum of 5a.

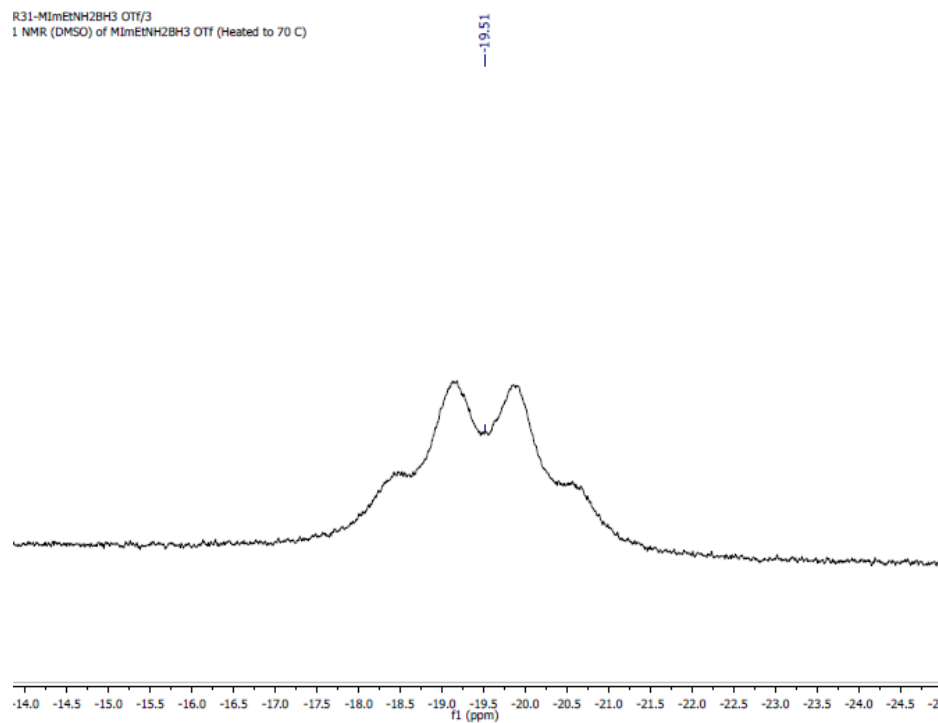


Fig S4. ¹¹B NMR spectrum of **5a**.

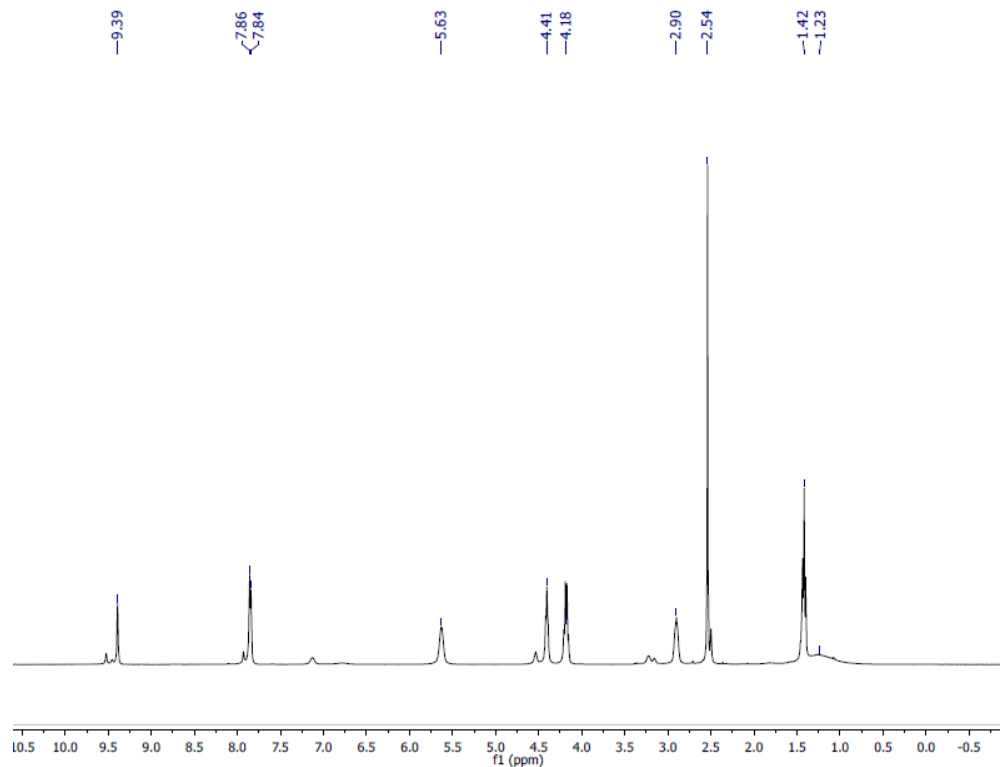


Fig S5. ¹H NMR spectrum of **4b**.

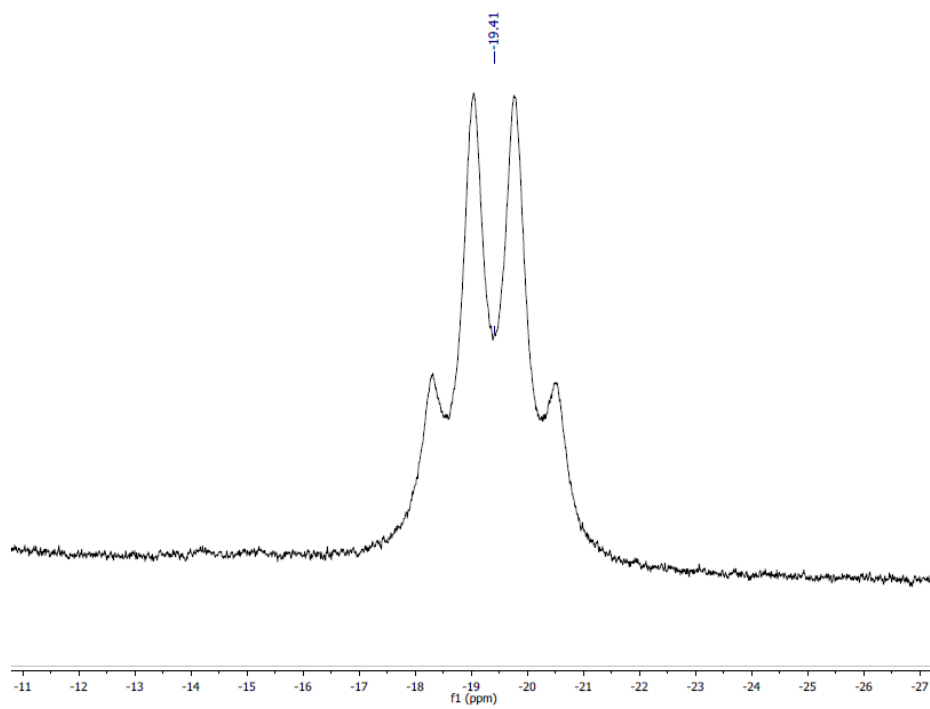


Fig S6. ^{11}B NMR spectrum of **4b**.

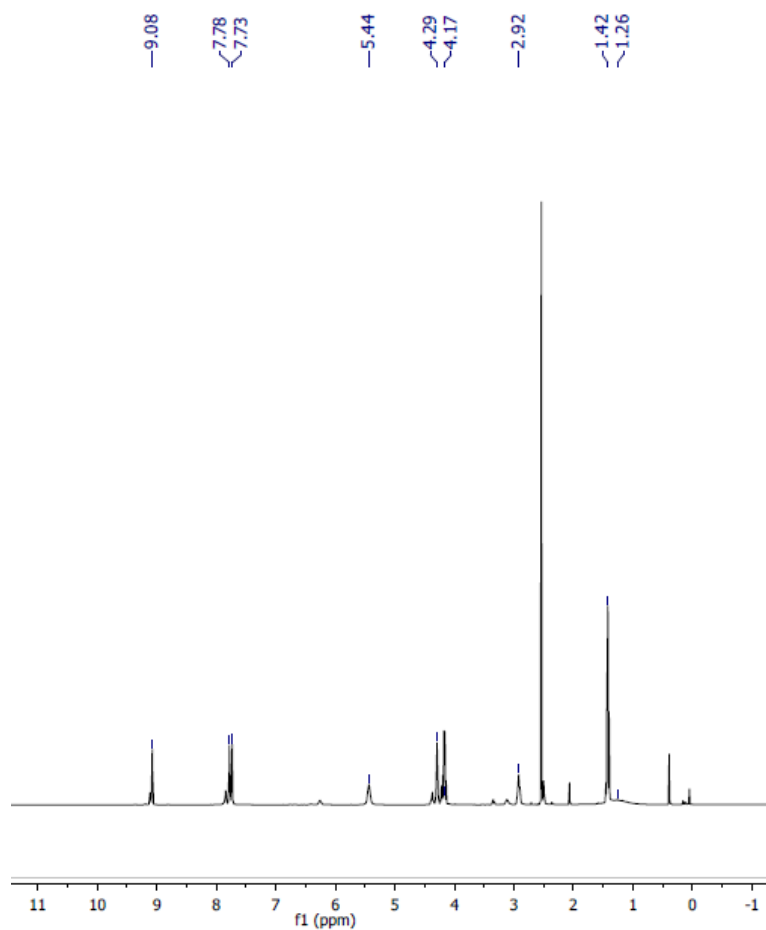


Fig S7. ^1H NMR spectrum of **5b**.

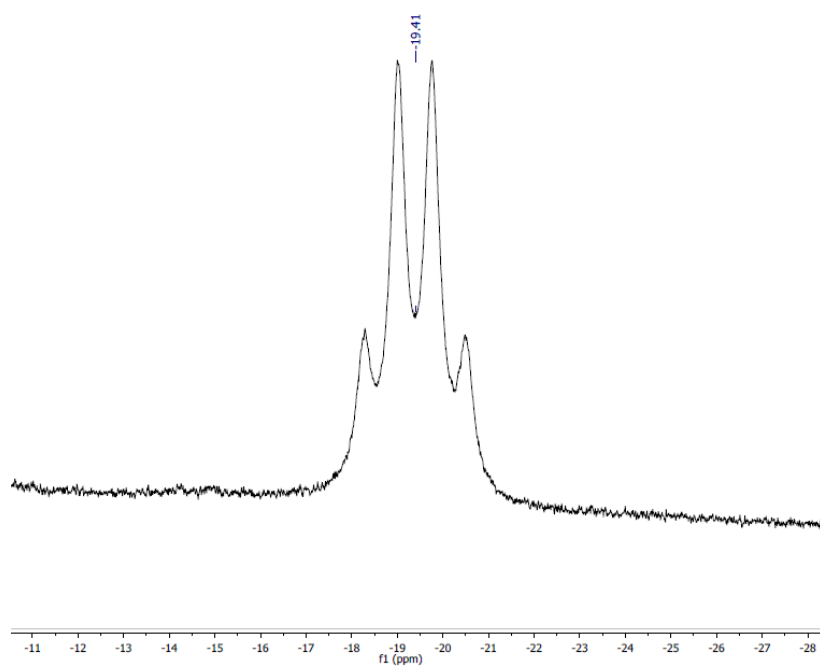


Fig S8. ^{11}B NMR spectrum of **5b**.

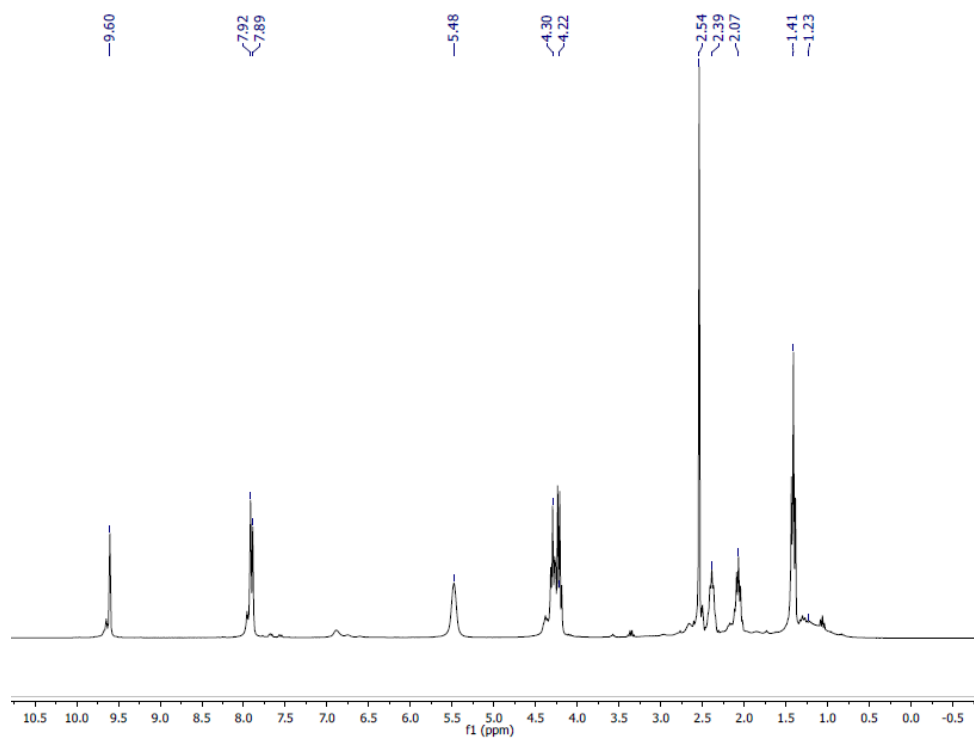


Fig S9. ¹H NMR spectrum of **4c**.

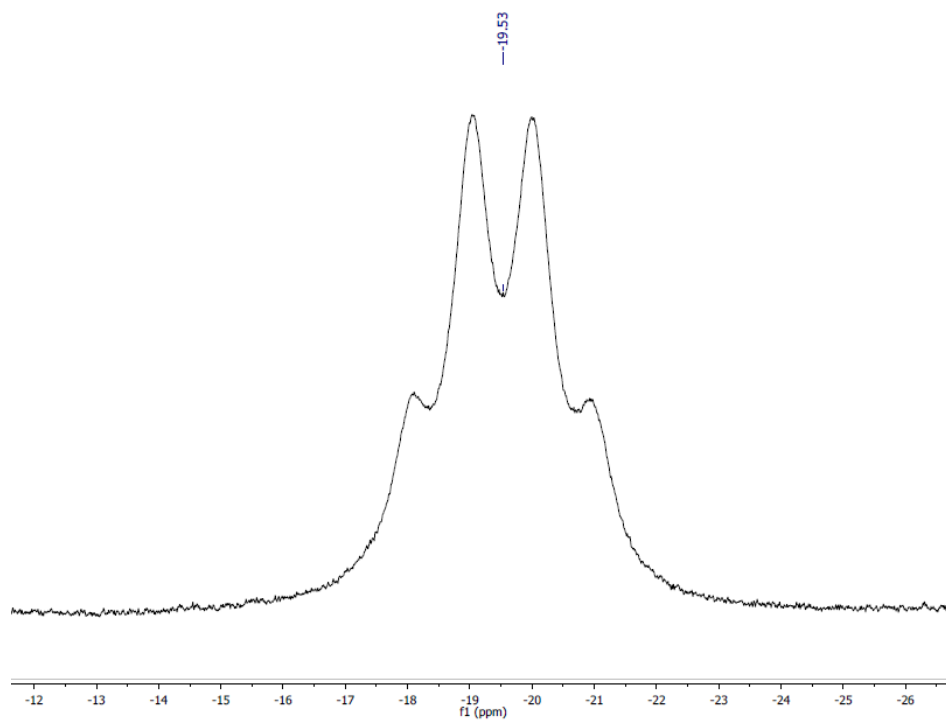


Fig S10. ¹¹B NMR spectrum of **4c**.

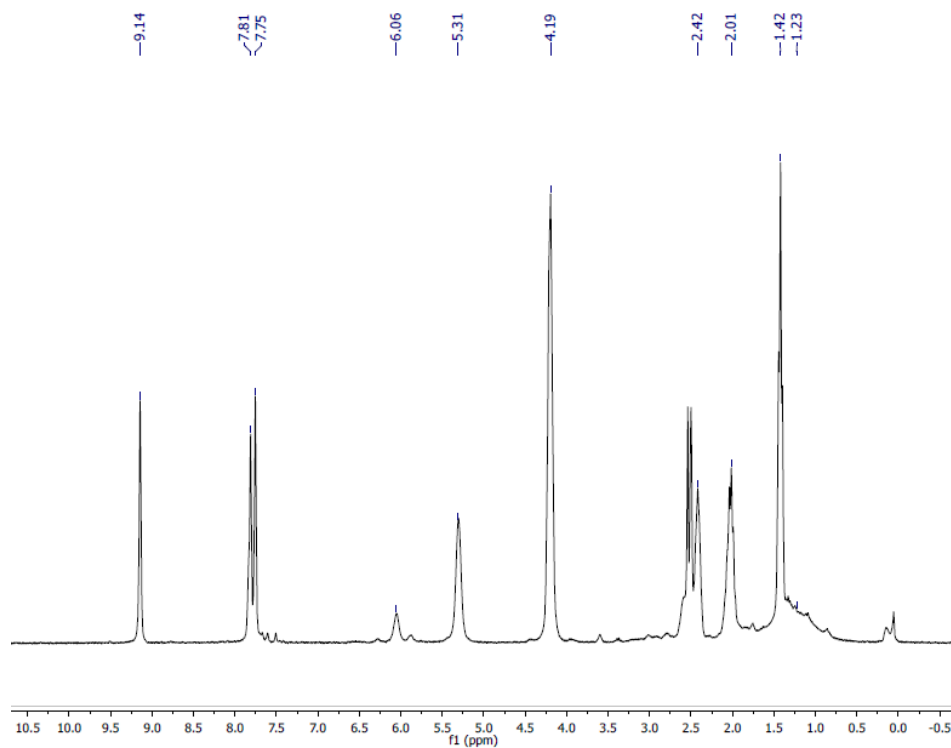


Fig S11. ¹H NMR spectrum of **5c**.

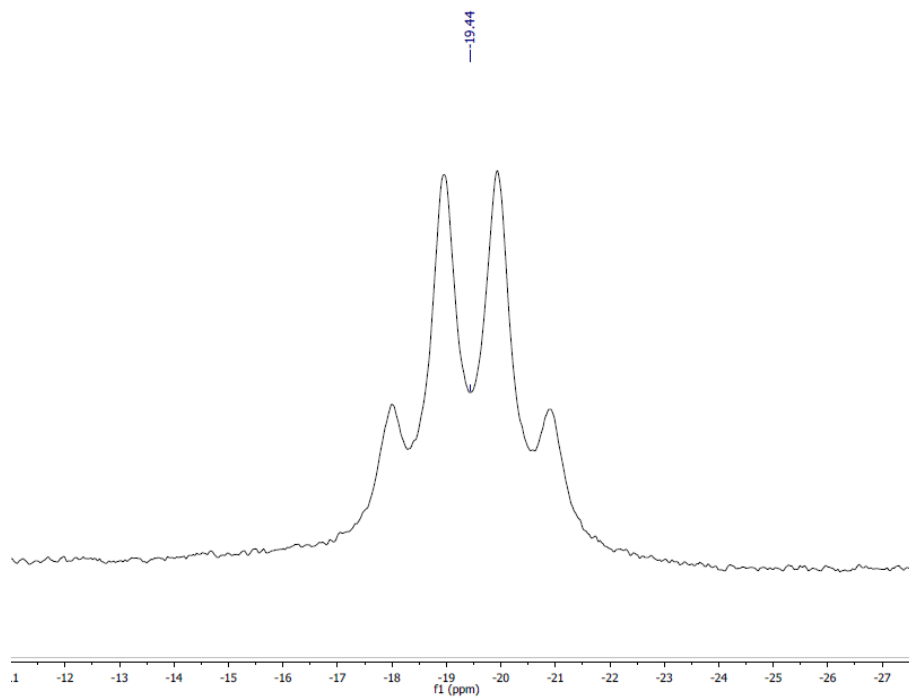


Fig S12. ¹¹B NMR spectrum of **5c**.

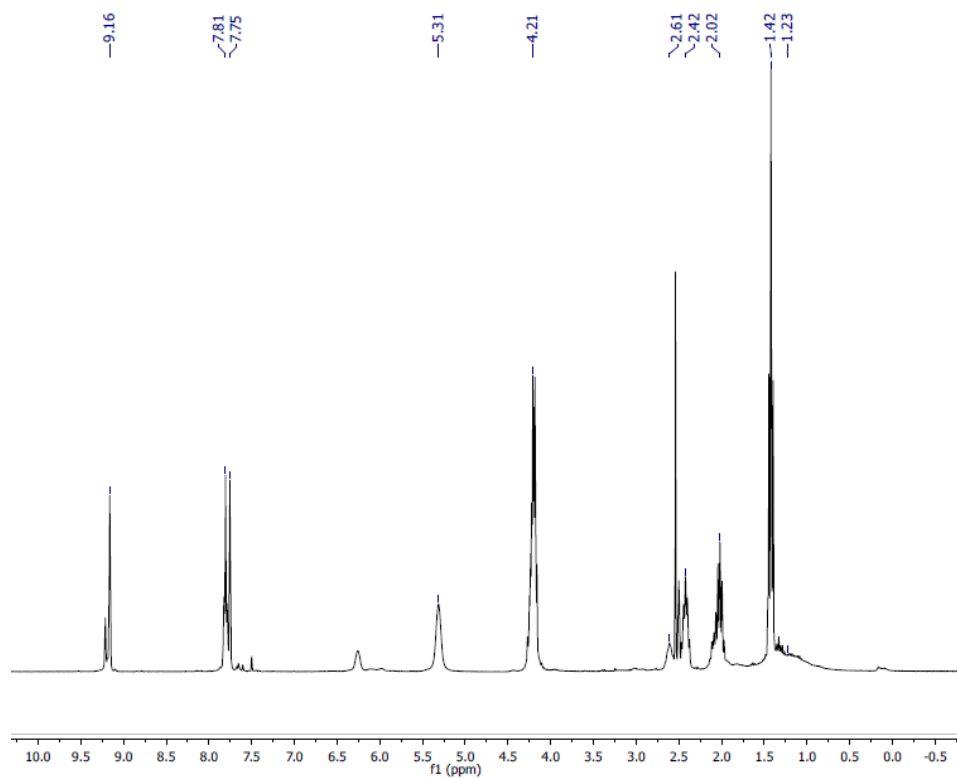


Fig S13. ¹H NMR spectrum of **6c**.

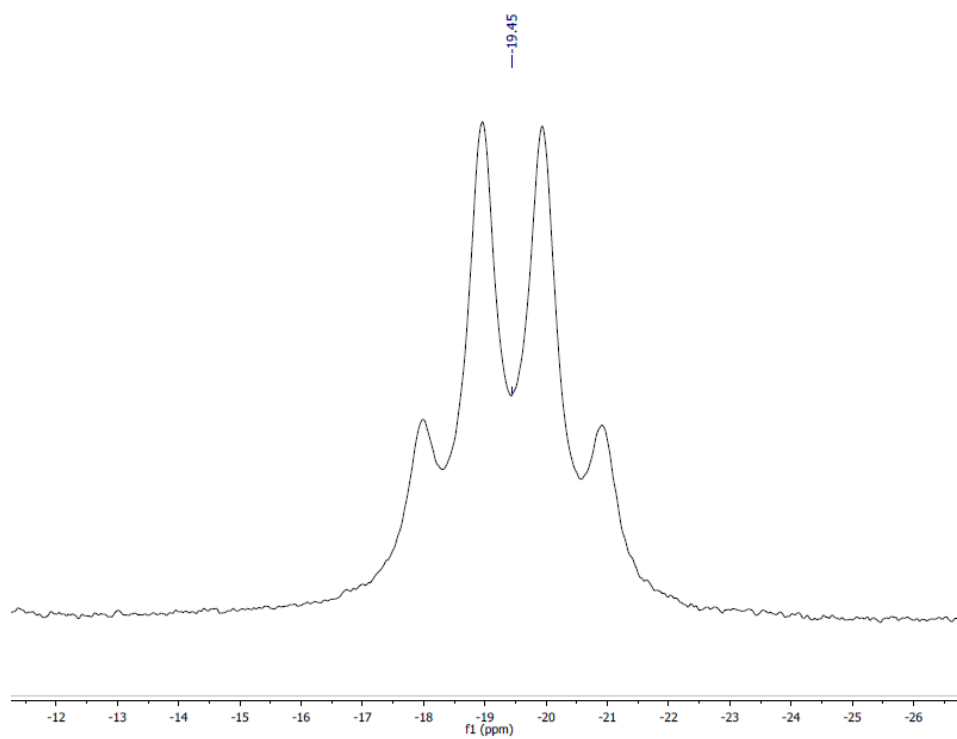


Fig S14. ¹¹B NMR spectrum of **6c**.

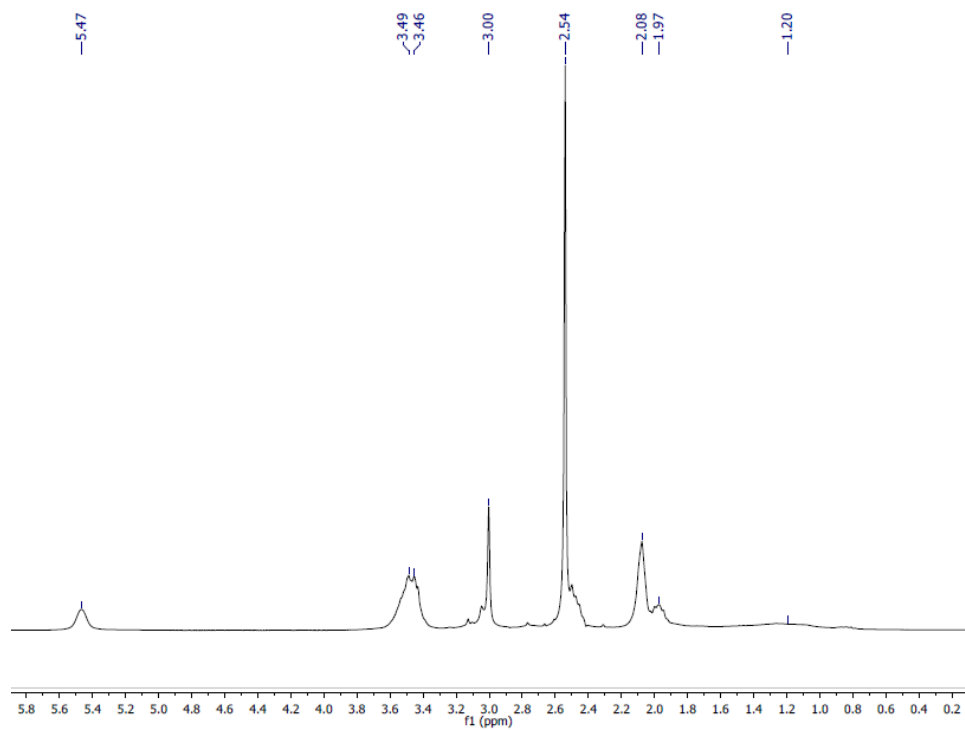


Fig S15. ¹H NMR spectrum of **4d**.

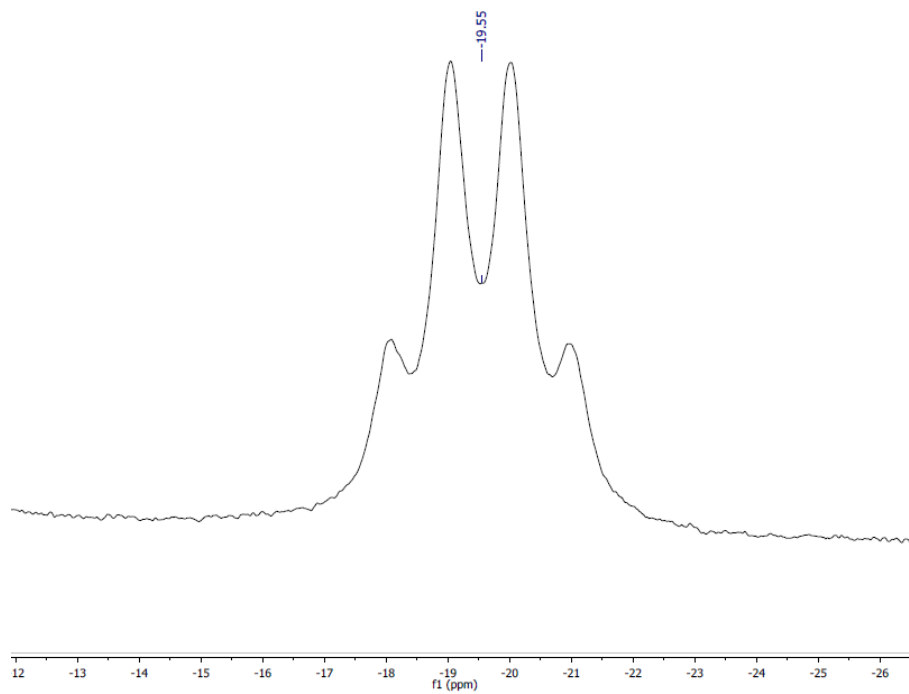


Fig S16. ¹¹B NMR spectrum of **4d**.

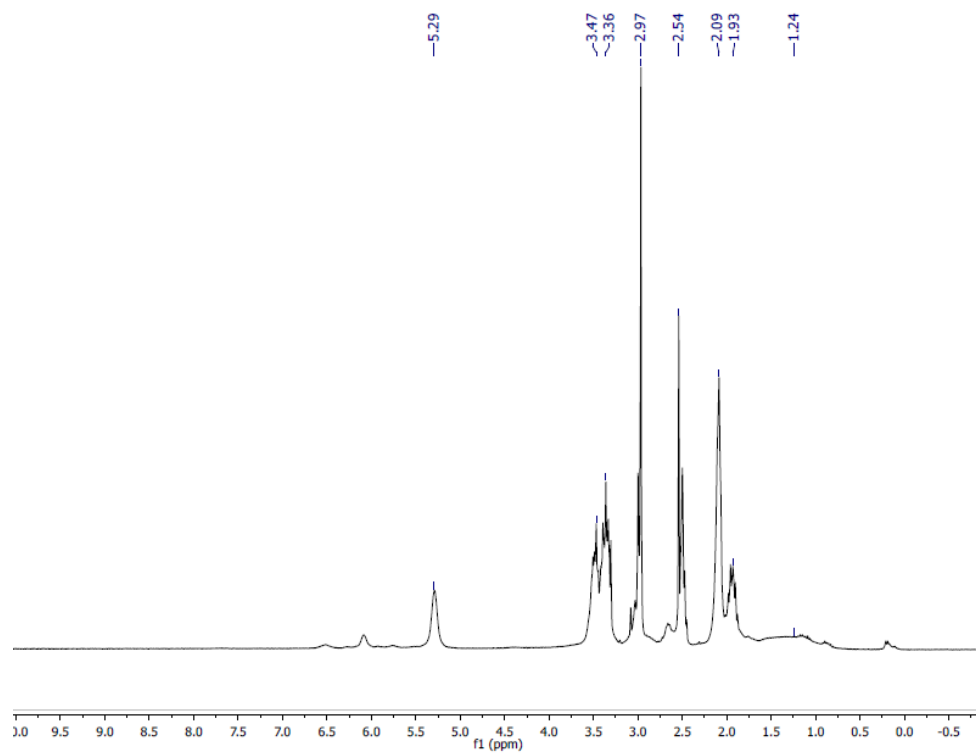


Fig S17. ¹H NMR spectrum of **5d**.

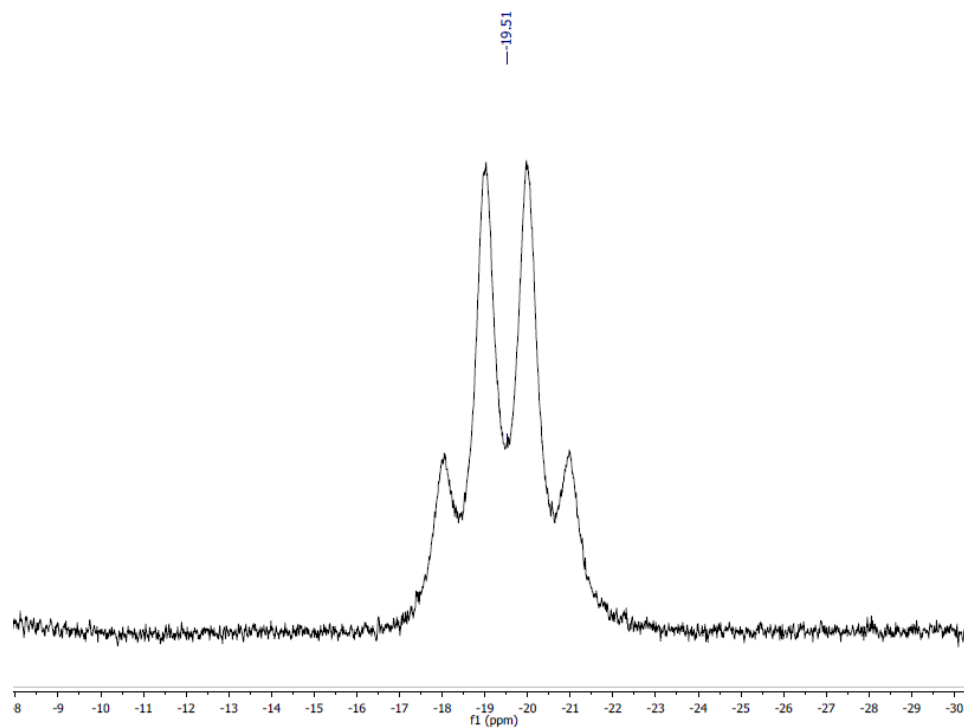


Fig S18. ¹¹B NMR spectrum of **5d**.

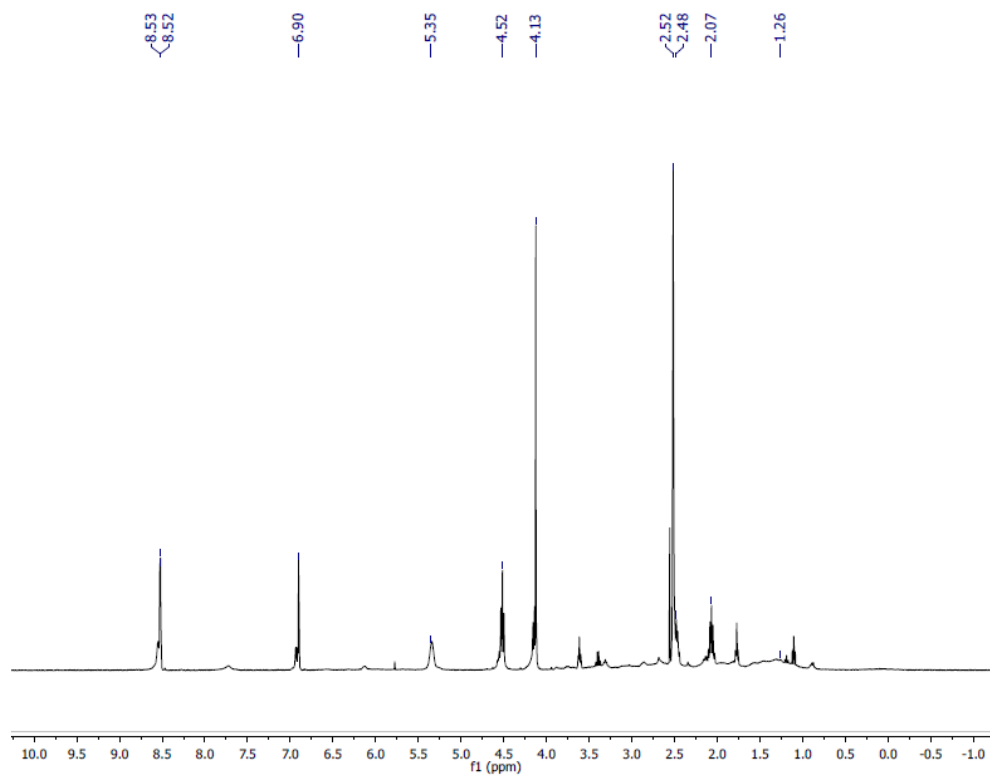


Fig S19. ^1H NMR spectrum of **4e**.

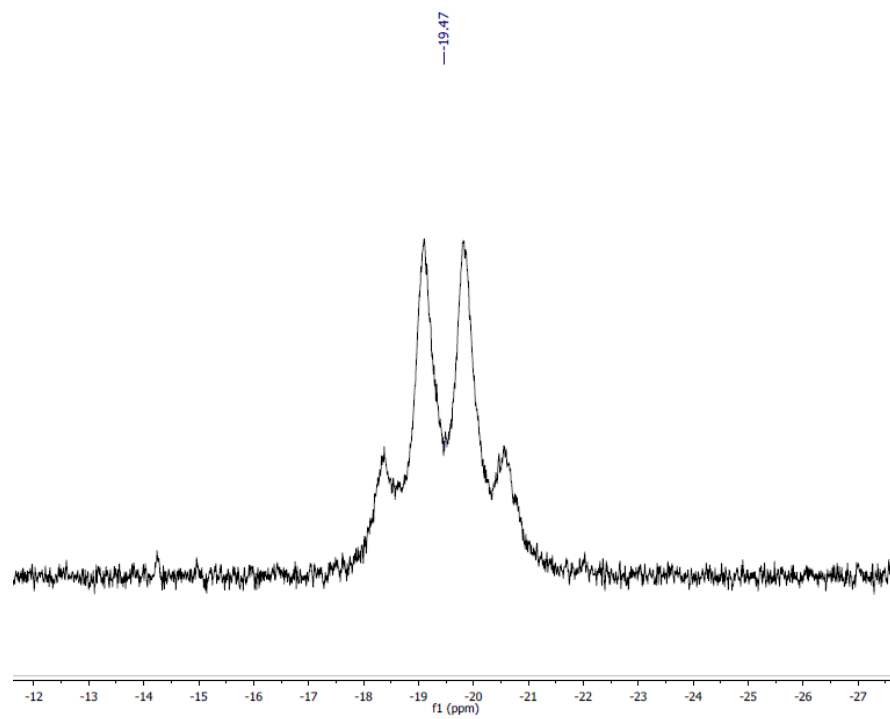


Fig S20. ^{11}B NMR spectrum of **4e**.

Table of dehydrogenation onset/max peak and integrated energy

| Compound | 1st Onset | 1st Max | 2nd Onset | 2nd Max | 3rd Onset | 3rd Max | $\Delta H_{\text{Dehydrogenation}}$ (kJ/mole) |
|---|-----------|---------|-----------|---------|-----------|---------|---|
| MeImEtAB Cl (4a) | 142.4 | 148.8 | | | | | -28.06 |
| MeImEtAB OTf (5a) | 81.3 | 90.1 | 92.7* | 100.3 | 134.1 | 140.6 | -41.08 |
| EtImEtAB Cl (4b) | 122.1 | 136.1 | 172.1* | 176.2 | | | -67.65 |
| EtImEtAB OTf (5b) | 88.0 | 122.4 | 130.2* | 134.9 | 182.2 | 203.8 | -50.25 |
| EtImPrAB Cl (4c) | 129.5 | 136.5 | 156.6* | 177.5 | | | -31.91 |
| EtImPrAB OTf (5c) | 85.7 | 103.2 | 113.4* | 114.3 | 133.0 | 139.0 | -43.99 |
| EtImPrAB NTf ₂ (6c) | 82.6 | 101.9 | 110.9* | 111.3* | | | -40.92 |
| MePyroPrAB Cl (4d) | 126.5 | 134.9 | 174.5 | 186.5 | | | -35.06 |
| MePyroPrAB OTf (5d) | 80.1 | 109.4 | 116.7* | 120.6 | | | -28.75 |
| MePyraPrAB Cl (4e) | 111.9 | 126.3 | 130.3* | 135.8 | | | -9.25 |

* = Onset unclear due to overlap with previous exo/endotherm. Value is where first noticeable deviation from the baseline is noticed.

Me = Methyl
Et = Ethyl
Pr = *n*-Propyl
AB = Amineborane

Im = Imidazolium
Pyro = Pyrrolidinium
Pyra = Pyrazolium

Cl = Chloride
I = Iodide
OTf = Triflate
NTf₂ = Bistriflimide

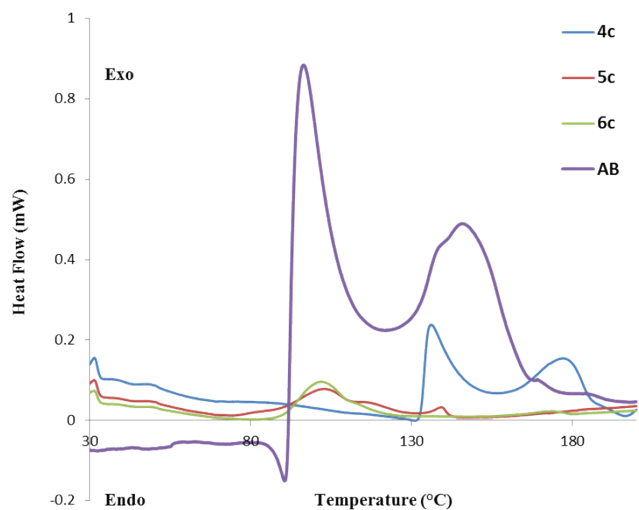


Fig S21 DSC traces of 1-ethyl-3-(*n*-propylaminoborane)-imidazolium with the chloride (N-ABIL 5), triflate (N-ABIL 6), bistriflimide (N-ABIL 7) anions and AB. Heat flow is normalized to 1 mg of material.

Head-space analysis (IR Spectra) from the dehydrogenation of

[EImPrNH₂BH₃]NTf₂, **6c** and **6c** + 2 AB

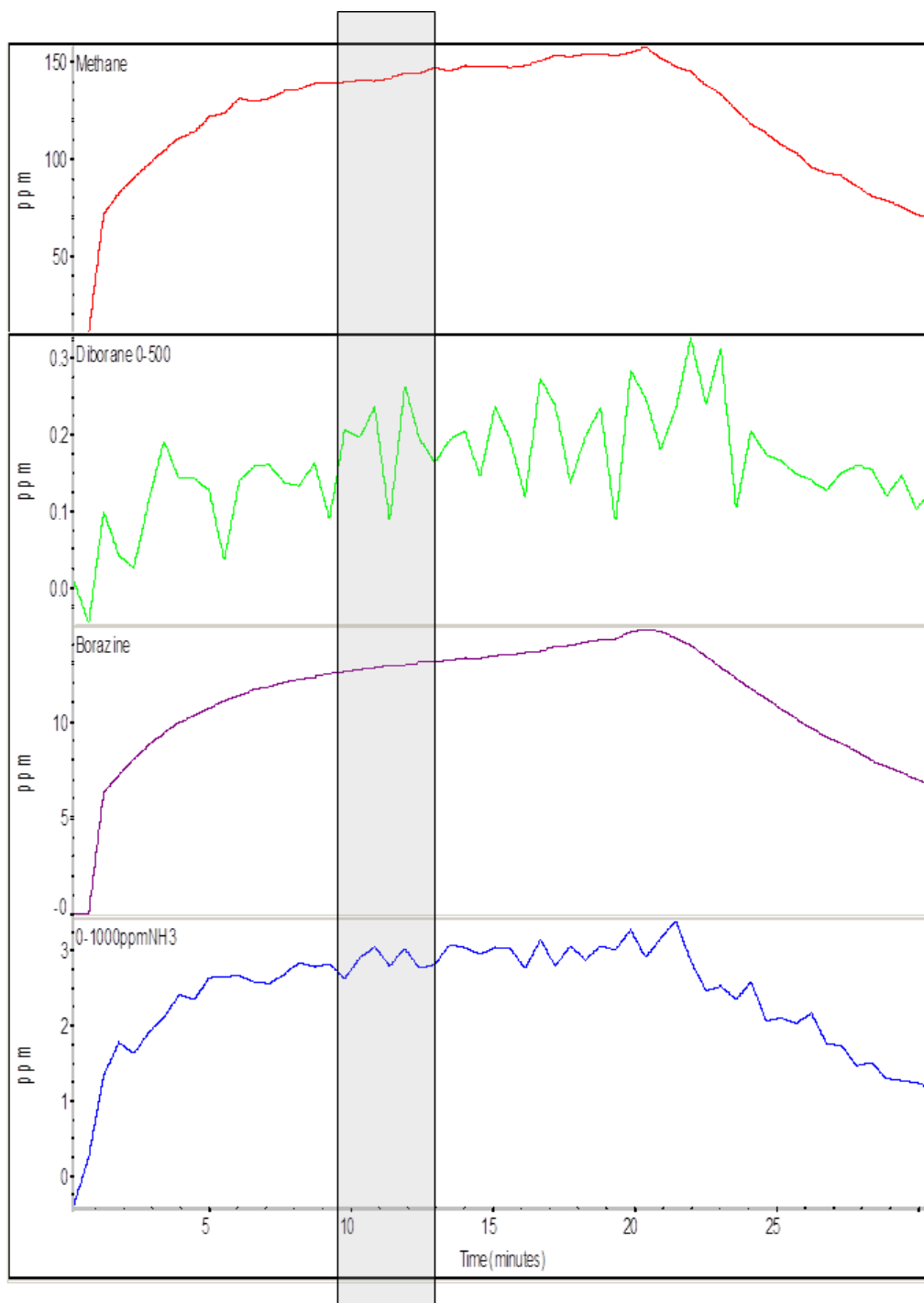


Fig. S22. Gas-phase IR measurements of trace gases produced in the rapid dehydrogenation of [EImPrNH₂BH₃]NTf₂ (**6c**).

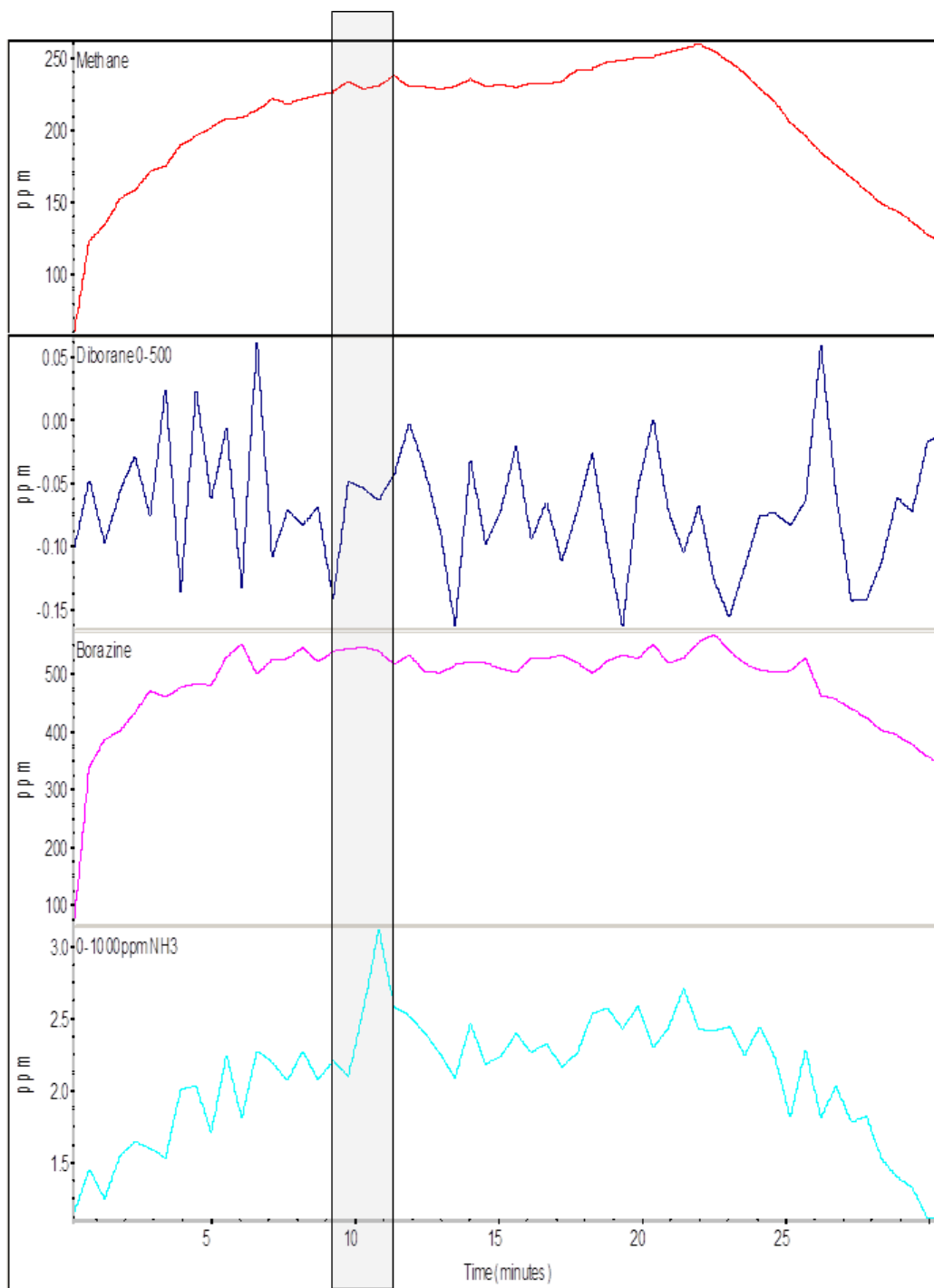


Fig. S23. Gas-phase IR measurements of trace gases produced in the rapid dehydrogenation of $[\text{ElmPrNH}_2\text{BH}_3]\text{NTf}_2$ (**6c**) blended with two equivalents of ammonia-borane.

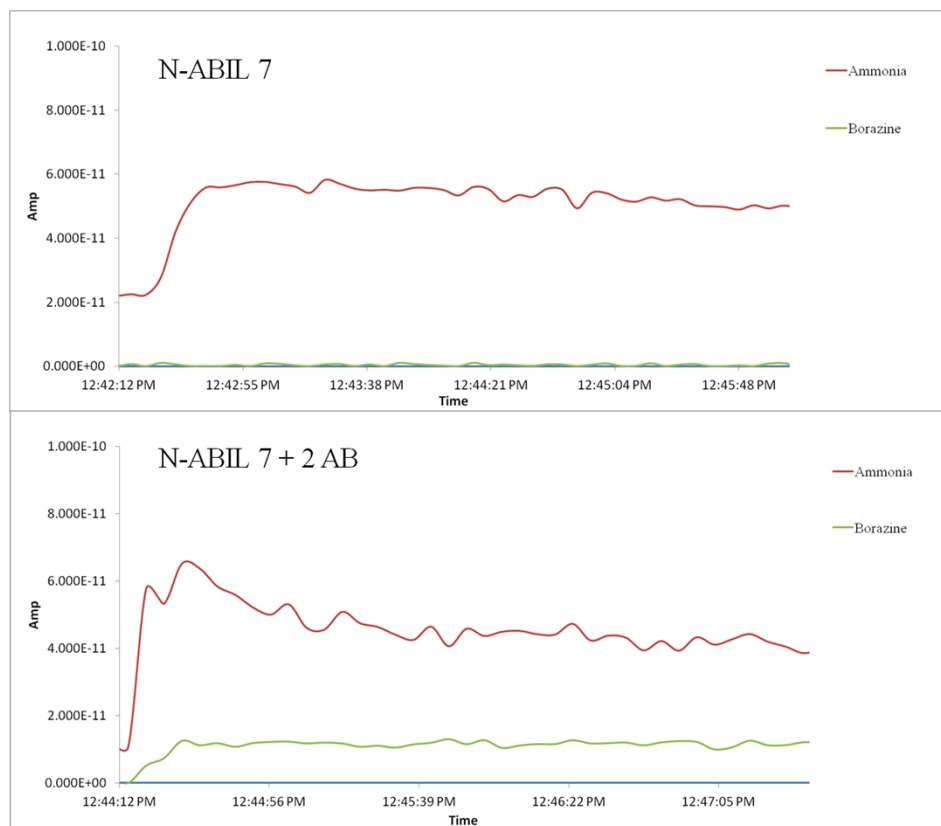


Fig. S24. Mass-spectra (quadrupole) of evolved gases from $[\text{EImPrNH}_2\text{BH}_3]\text{NTf}_2$ (top) and $[\text{EImPrNH}_2\text{BH}_3]\text{NTf}_2$ blended with 2 equivalents of AB (bottom). Diborane is not shown due to overlap with the carrier gas (N_2).

ESI-Mass spectra of compounds of 4a, 6c, and 4e, as well as the post dehydrogenation product of 6c

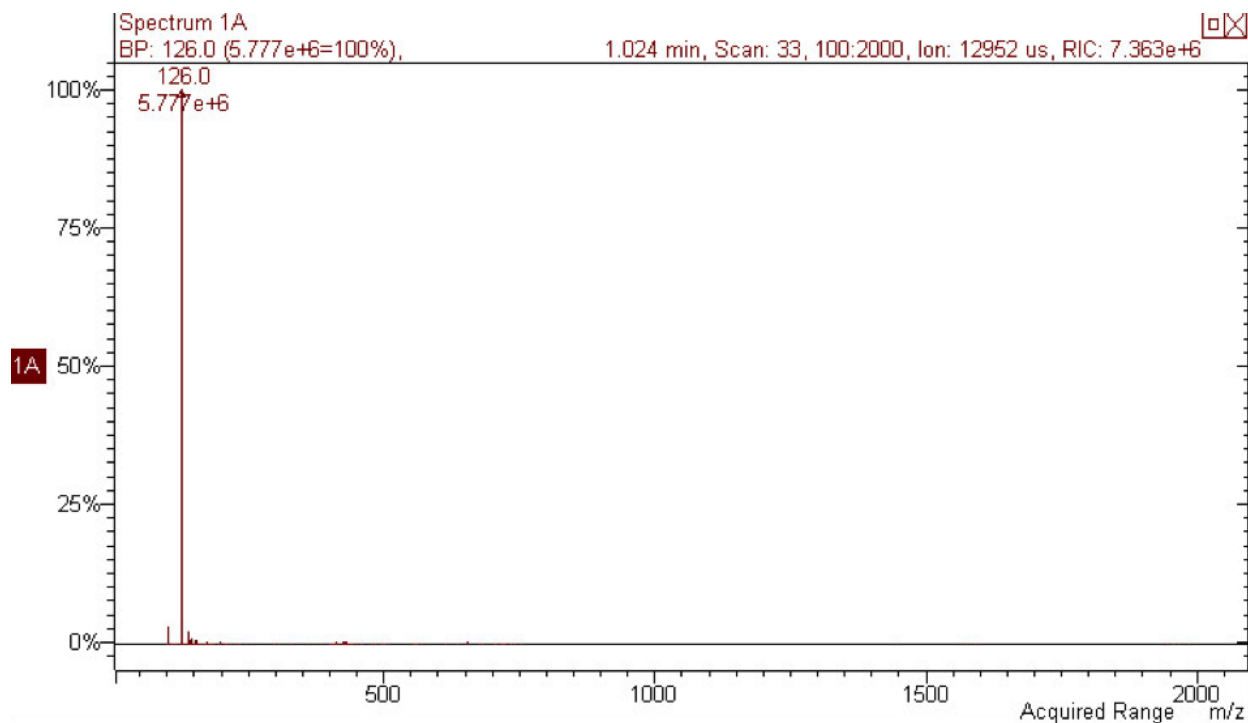


Fig S25. Positive ESI-MS of **4a**. The signal is representative of cation where the BH₃ moiety removed.

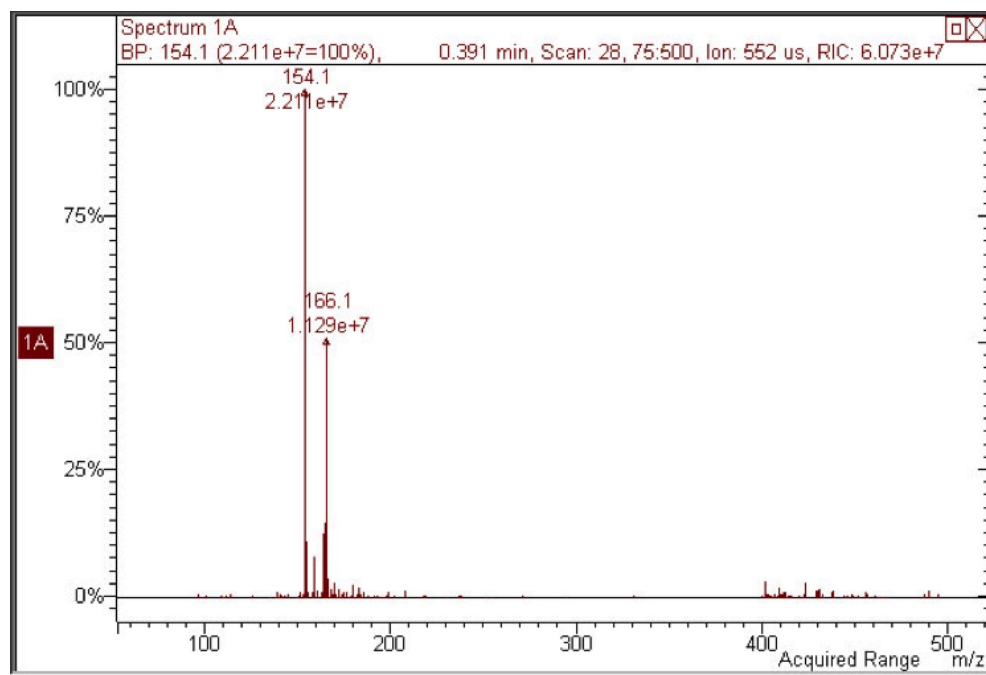


Fig S26. Positive ESI-MS of **6c** with optimization plot. Largest signal at 154.1 m/z is characteristic of the cation losing BH₃.

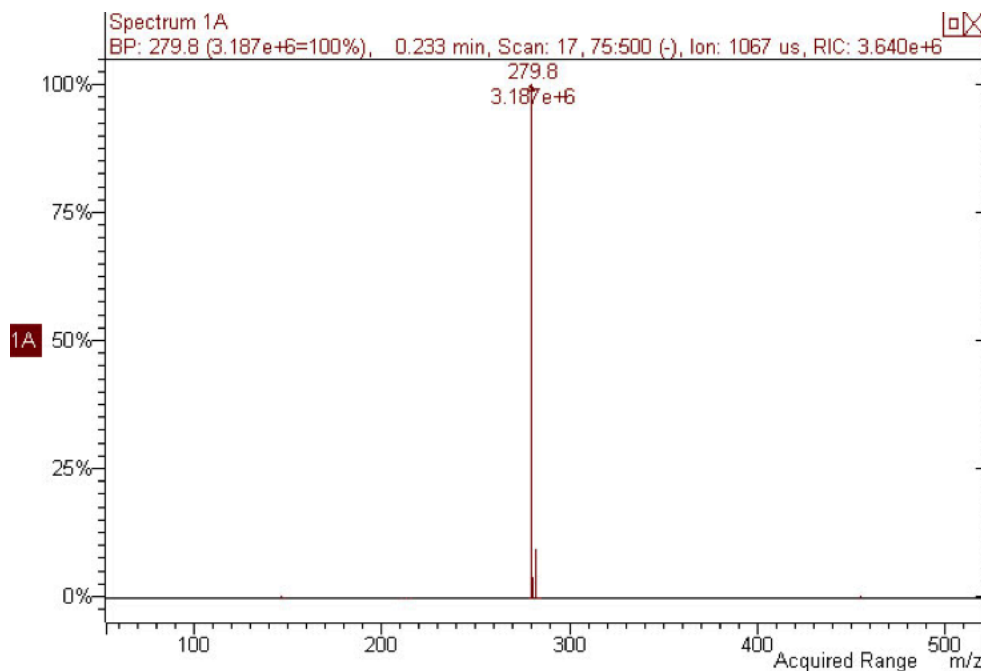


Fig S27. Negative ESI-MS of **6c** with optimization plot. Largest signal 279.8 m/z is characteristic of the bistriflimide anion.

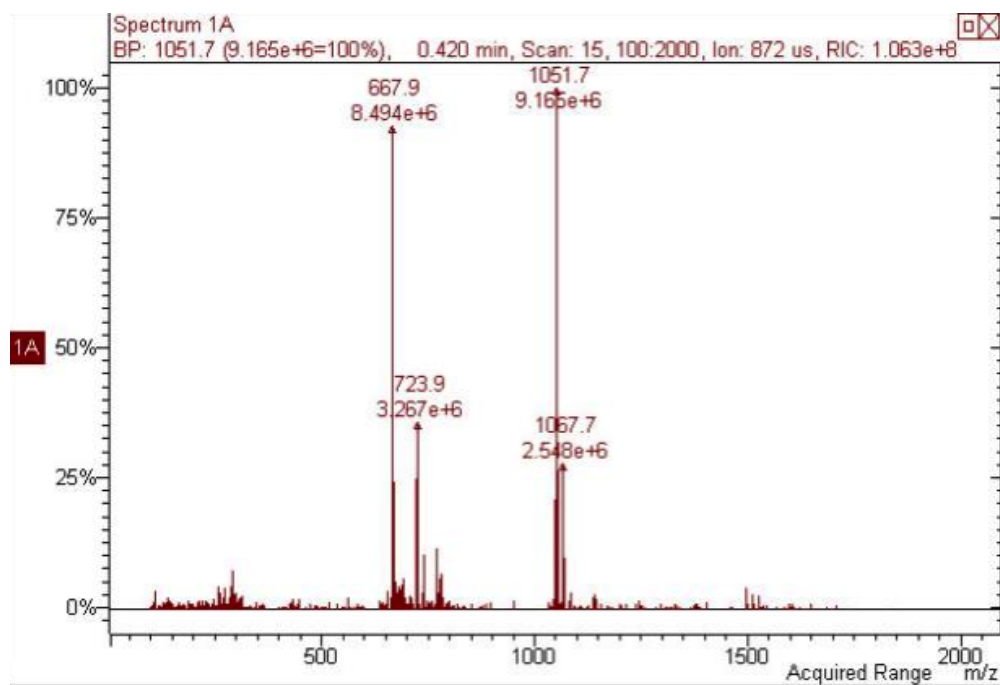


Fig S28. Positive ESI-MS of dehydrogenated N-ABIL 7 (**6c**). The trimer becomes obvious due to the signal at m/z =1051.7, resulting from the loss of one NTf₂ anion. The second major signal

likely originates from a long chain oligomer with missing NTf_2 anions. It should be noted that the signal at $m/z = 667.9$ is not present when N-ABIL 7 is blended with AB, demonstrating its susceptibility towards oligomerization.

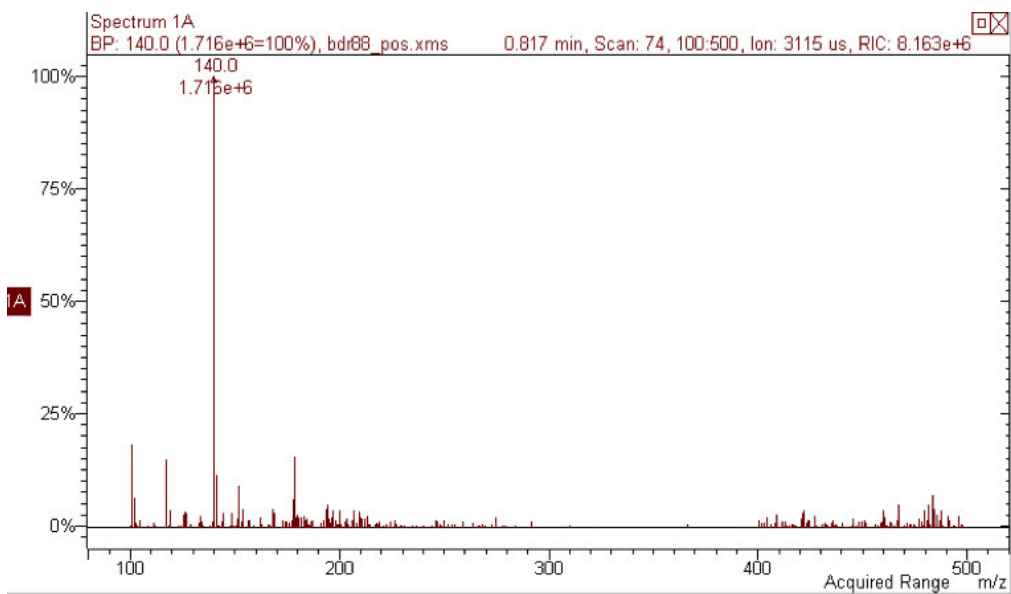


Fig S29. Positive ESI-MS and optimization plot of the dehydrogenation of N-ABIL 10 (**4e**). The largest signal at 140.0 m/z is characteristic of the cation losing BH_3 .

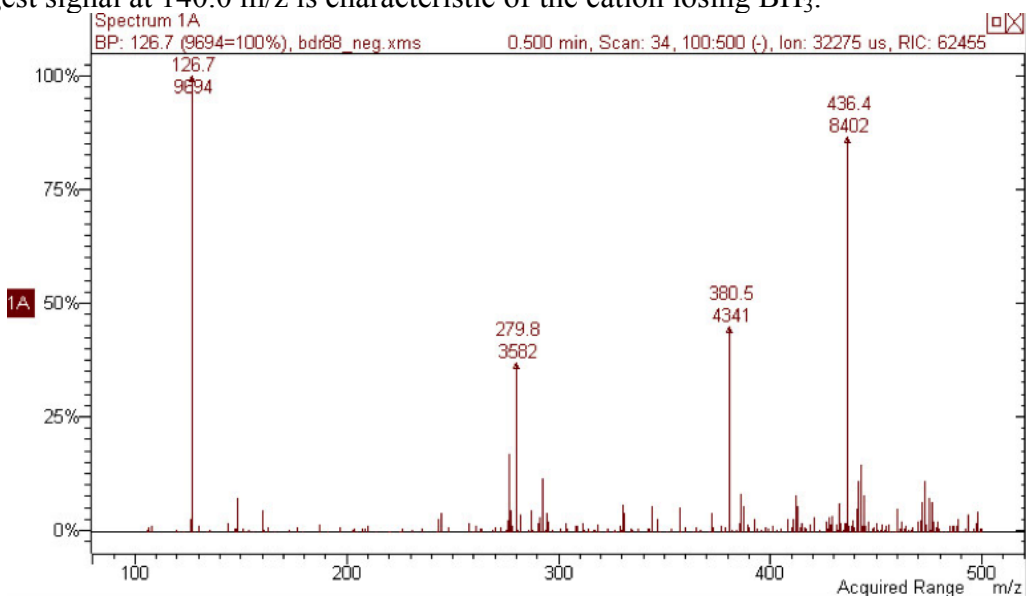


Fig S30. Negative ESI-MS and optimization plot of the dehydrogenation of N-ABIL 10 (**4e**). Signals at 126.7 and 380.5 are representative of the iodide and triiodide anions, respectively. The low counts, relative to the counts seen in the cation (1.7×10^6 counts), confirms that the major anion in the product is the chloride and that the iodide is removed during the purification steps.

X-ray crystallographic data, collection parameters, and thermal ellipsoid plots¹ for 2a and 3b

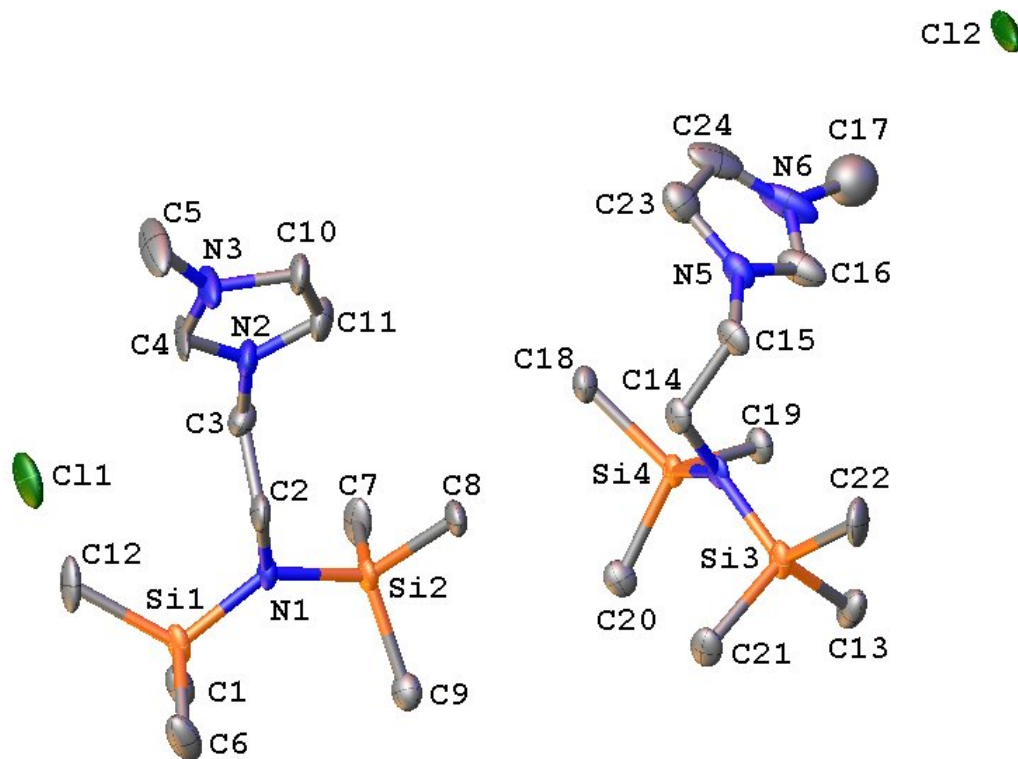


Fig. S31. Thermal ellipsoid plot (30%) of **2a**. Hydrogen atoms removed for clarity.

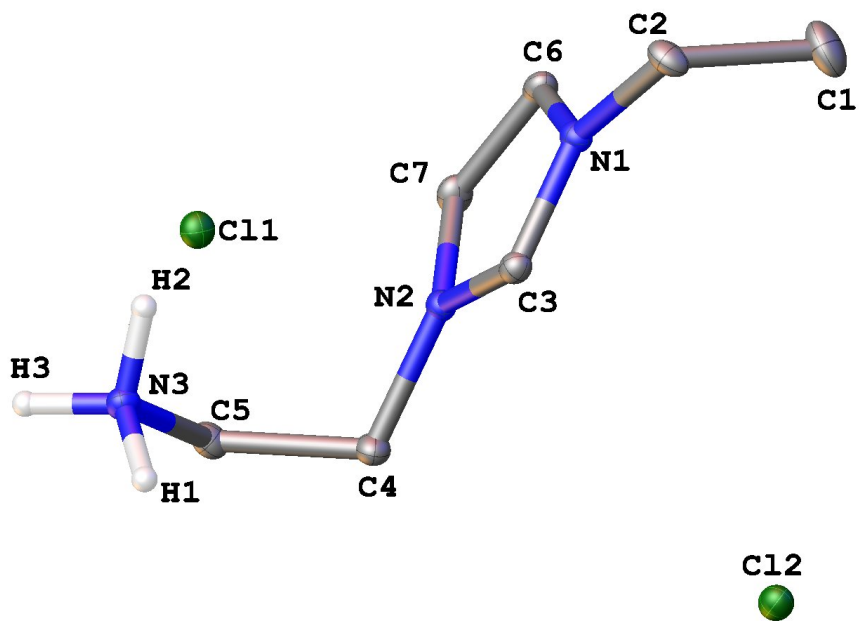


Fig. S32. Thermal ellipsoid plot (30%) of **3b**. Aside from ammonium protons, hydrogen atoms are removed for clarity.

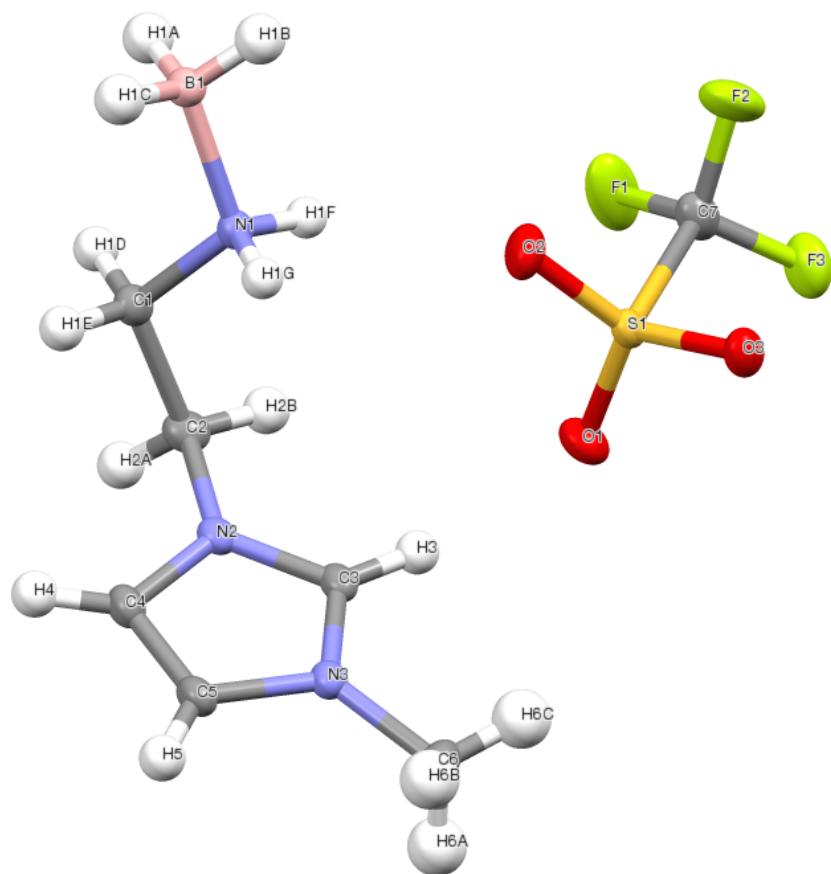


Fig. S33. Thermal ellipsoid plot (30%) of **5a**.

Crystallographic methods

Crystals of **2a**, **3b**, and **5a** were mounted in a nylon cryoloop from Paratone-N oil. The data were collected on a Bruker D8 diffractometer, with APEX II charge-coupled-device (CCD) detector, and Bruker Kryoflex liquid N₂ low temperature device (140 K). The instrument was equipped with graphite monochromatized MoK α X-ray source ($\lambda = 0.71073$ Å), and a 0.5 mm monocapillary. A hemisphere of data was collected using ω scans, with 10-second frame exposures and 0.5° frame widths. Data collection and initial indexing and cell refinement were handled using APEX II¹ software. Frame integration, including Lorentz-polarization corrections, and final cell parameter calculations were carried out using SAINT⁺² software. The data were corrected for absorption using redundant reflections and the SADABS³ program. Decay of reflection intensity was not observed as monitored *via* analysis of redundant frames. The structure was solved using Direct methods and difference Fourier techniques. All hydrogen atom positions were idealized, and rode on the atom they were attached to. The final refinement included anisotropic temperature factors on all non-hydrogen atoms. Structure solution, refinement, graphics, and creation of publication materials were performed using SHELXTL⁴.

Disorder in the chloride anion positions, and the imidazolium methyl group was observed in **2a**. These positions were refined in two partial occupancy positions using a set occupancy factor of 0.5 for the methyl group, and variable occupancy factors tied to 1.0 for the chloride positions. For C11 site occupancy factors refined to 0.63(3), and 0.32(3), and for Cl2 final site occupancy factors were 0.69(2) and 0.31(2).

References

1. APEX II 1.08, **2004**, Bruker AXS, Inc., Madison, Wisconsin 53719.
2. SAINT+ 7.06, **2003**, Bruker AXS, Inc., Madison, Wisconsin 53719.
3. SADABS 2.03, **2001**, George Sheldrick, University of Göttingen, Germany.
4. SHELXTL 5.10, **1997**, Bruker AXS, Inc., Madison, Wisconsin 53719.